

MIMO FSO Systems in Hybrid Quantum Noise Environments: SKR Analysis with One- and Two-way CV-QKD Protocols

Sushil Kumar, Soumya P. Dash, *Senior Member, IEEE*, and George C. Alexandropoulos, *Senior Member, IEEE*

Abstract—This paper studies a multiple-input multiple-output (MIMO) free-space optical (FSO) communication system employing continuous-variable quantum key distribution (CV-QKD), with the goal to support secret key transmission between two legitimate users, Alice and Bob. All involved wireless channels are subjected to atmospheric turbulence leading to beam spreading, pointing error, and turbulence-induced fading, which along with the presence of hybrid quantum noise negatively impact secret key exchange. Furthermore, the legitimate MIMO FSO system faces the threat of compromise from an eavesdropper, Eve, employing a collective Gaussian attack to intercept the secret key exchange. Novel one- and two-way protocols for enhancing the security of the transmitted keys are proposed. To this end, the transmissivity of the FSO channels is mathematically formulated and bounds on the mutual information between the transmitted and received coherent states are obtained, which are then used for deriving novel expressions for the secret key rates (SKRs) for both one- and two-way protocols. The presented numerical results corroborate the proposed analytical secrecy framework, quantifying the SKR gains obtained by employing MIMO and the two-way protocol for FSO CV-QKD systems.

Index Terms—One-way and two-way protocols, continuous variable quantum key distribution, free-space optical communications, hybrid quantum noise, MIMO, secret key rate.

I. INTRODUCTION

The upcoming sixth-generation (6G) communication networks are expected to provide seamless connectivity anytime and anywhere [1], [2]. This goal motivates the integration of non-terrestrial networks (NTNs), encompassing satellite-based systems and high-altitude platforms, with terrestrial infrastructures, which is lately receiving substantially research and development interests [3]–[6]. Free-space optical (FSO) communication systems constitute the most prominent enabling technology to support such networks, due to their ability to deliver high-capacity, interference-resistant, and license-free links with rapid deployment over extensive distances [7]–[9]. However, their deployment over multiple operators and in dynamic topologies inherently leads to the demand for secure data transmissions in the presence of eavesdroppers that compromise legitimate data traffic integrity.

Several studies in the literature have explored the use of classical cryptographic techniques to enhance the security of data transmission in FSO-based systems [10]–[13]. The available algorithms base their strength in extensive computational

complexity, making them practically infeasible to break using conventional computing resources within reasonable time frames. However, with the rapid advancements in quantum computing, particularly through Shor’s and Grover’s algorithms, encryption schemes, such as Rivest–Shamir–Adleman (RSA) and elliptic curve cryptography (ECC), are expected to become vulnerable, as their decryption can be achieved in significantly shorter time [14], [15]. This impending threat has motivated the exploration of alternative approaches for achieving unconditional security, among which quantum key distribution (QKD) has emerged as a promising solution [16], [17]. This scheme exploits fundamental principles of quantum mechanics, namely the no-cloning theorem and measurement disturbance, to enable two parties to securely exchange encryption keys, ensuring a level of security that remains impervious to potential advances in computational power [18]–[21].

Among the different categories of QKD protocols, continuous-variable QKD (CV-QKD), which encodes information onto the quadratures of coherent or squeezed states, presents as a viable technology for FSO systems [22]–[24], owing to its advantages including compatibility with standard optical telecommunication components, potentially higher secret key rates (SKR), and improved resilience to photon loss [25]. In [26], the authors analyzed the transmission characteristics of QKD over a single-input single-output (SISO) FSO channel, focusing on the impact of atmospheric turbulence on the overall transmission probability. Extending this line of research, [27] examined the feasibility of distributing CV-QKD-encoded secret keys from a satellite platform to multiple legitimate ground users, thereby addressing the scalability of QKD for satellite networks. Furthermore, [28] investigated the achievable SKR for a SISO FSO link assisted by an unmanned aerial vehicle, where CV-QKD was employed to enhance secure communications in dynamic airborne environments. To mitigate the fractional loss of secret keys caused by the lengthy and complex reconciliation process in one-way QKD, a two-way QKD protocol, leveraging bidirectional communication between the legitimate transceiver pair, was introduced in [29] and later applied in [30] to enhance the secrecy performance in SISO FSO systems.

Most current FSO QKD studies focus on SISO configurations, whose performance is limited by atmospheric disturbances that can deflect or spread the beam, sometimes causing it to miss the receiver’s aperture entirely, resulting in connection failure. In addition to these propagation impairments, secret key transmission in FSO systems is further degraded by quantum noise [31]. Such noise originates from environmental interactions, qubit coupling, and imperfect system controls, leading to dephasing and decoherence. Alongside classical

S. Kumar and S. P. Dash are with the School of Electrical and Computer Sciences, Indian Institute of Technology Bhubaneswar, Argul, Khordha, 752050 India, (e-mails: {a24ec09010, spdash}@iitbbs.ac.in).

G. C. Alexandropoulos is with the Department of Informatics and Telecommunications, National and Kapodistrian University of Athens, Panepistimiopolis Ilissia, 16122 Athens, Greece and also with the Department of Electrical and Computer Engineering, University of Illinois Chicago, IL 60601, USA (e-mail: alexandg@di.uoa.gr).

noise, quantum noise can significantly degrade quantum channel fidelity and compromise communication reliability.

To mitigate the adverse effects of channel propagation and fading, multiple-input multiple-output (MIMO) techniques have been recently integrated with CV-QKD, demonstrating notable improvements in the system's performance [19], [24], [32], [33]. Furthermore, it was shown in [34] that employing two-way communication protocols in MIMO FSO systems can further enhance SKR performance. However, existing studies predominantly assume simplified noise models, limiting their applicability to practical FSO scenarios. Moreover, [34] showcased that implementing the two-way communication protocol for MIMO FSO systems improves their SKR performance.

However, to the best of our knowledge, the performance of one- or two-way protocols for such MIMO FSO systems subject to hybrid quantum noise has not been analyzed. In fact, MIMO-assisted CV-QKD under the two-way protocol remains significantly under-explored. Specifically, most studies tend to overlook the simultaneous effects of discrete photon noise and continuous thermal noise. This coexistence is unavoidable in practical FSO receivers operating in the presence of background radiation and imperfect detection, and the presence of hybrid quantum noise is expected to directly impact mutual information and SKR in MIMO systems, where noise accumulation and spatial correlations can significantly affect system performance [35]. Motivated by these limitations, this paper addresses these research gaps by considering a MIMO FSO system in which two legitimate users, Alice and Bob, attempt to achieve secure secret key exchange in the presence of an eavesdropper, Eve, who compromises the system's security by employing a collective Gaussian attack. The FSO channels are considered to degrade the secret-key transmission achieved via CV-QKD due to atmospheric turbulence, which causes diffraction, spreading, and misalignment of the transmitted beams, and due to the presence of hybrid quantum noise. The main contributions of this paper are summarized as follows:

- By accounting for the beam spreading occurring during transmission, which is modeled by considering the field distribution of the beams at the transceiver pair, the pointing error of the beams, which is modeled by the Weibull distribution, and the turbulence-induced fading, modeled by the lognormal distribution, a mathematical framework for the transmissivity of the considered MIMO FSO configuration is presented.
- A one- and a two-way protocols for the considered MIMO FSO CV-QKD system when operating under hybrid quantum noise, modeled by a Gaussian mixture distribution guided by a Poisson process, are proposed.
- Novel analytical expressions for the SKR performance of the considered system with both presented protocols and for the case where Bob's receiver utilizes homodyne detection along with reverse reconciliation (RR), while the eavesdropper employs collective Gaussian attack for data decryption, are presented.
- The superiority of the two-way protocol over its one-way counterpart, along with the SKR enhancement achieved through the MIMO configuration with respect to SISO, is showcased through an asymptotic analysis.

The rest of the paper is organized as follows. Section II presents the MIMO FSO CV-QKD system model, detailing the channel model, the analytical framework for channel transmissivity, and the additive hybrid quantum noise model. The transmission and reception of the secret keys, along with the effect of the collective Gaussian attack by the eavesdropper, are described for the one- and the two-way protocols in Section III. Capitalizing on the statistics of the hybrid quantum noise, Section IV proposes bounds on the mutual information between the transmitted and received states for both considered protocols, which are then utilized, in Section V, to derive closed-form and asymptotic expressions for the SKR performance. The numerical results corroborating the analytical findings and showcasing the dependency of the system performance on the considered parameters are presented in Section VI. Finally, Section VII presents the concluding remarks of the paper.

Notation: \mathbf{A}^\dagger and \mathbf{A}^T denote the conjugate transpose and transpose of a matrix \mathbf{A} , respectively. $\mathbf{1}_N$, $\mathbf{0}_N$, and \mathbf{I}_N represent a $1 \times N$ vector of ones, the $N \times N$ zero matrix, and the $N \times N$ identity matrix, respectively. $J_0(\cdot)$ denotes the zero-order Bessel function of the first kind, $j \triangleq \sqrt{-1}$, and $\text{diag}(\mathbf{a})$ constructs an $M \times M$ diagonal matrix with the elements of vector \mathbf{a} along its principal diagonal. We also use the definition $\mathbf{Z} \triangleq \text{diag}(1, -1)$. The operator \otimes represents the Kronecker product, while $\mathbf{E}[\cdot]$ and $\langle X \cdot Y \rangle$ denote the expectation operator and the quantum correlation between X and Y , respectively. Finally, \hat{Q} denotes an operator (such as annihilation or creation) acting on the signal mode Q . Furthermore, $\mathcal{N}(\mu, \sigma^2)$ denotes a real Gaussian random variable with a mean value of μ and variance of σ^2 .

II. SYSTEM MODEL

The considered CV-QKD system, illustrated in Fig. 1, consists of a MIMO FSO channel between two legitimate users, namely, Alice and Bob, equipped with N_T and N_R optical transceivers (or sub-apertures), respectively. Typically, laser sources (LSs) are employed for the transmission phase, and photodetectors (PDs) are used for the detection process. Alice and Bob aim to establish a successful exchange of secret keys using the CV-QKD scheme in the presence of an eavesdropper, Eve, who is targeting to steal the secure information.

A. Channel Model

The FSO channels are subjected to atmospheric turbulence that leads to diffraction, spreading, and misalignment of the transmitted beams. Thus, we denote the MIMO FSO channel gain matrix by $\mathbf{H} \in \mathbb{C}^{N_R \times N_T}$, with the spatial sub-channel between the j -th transmit aperture and the l -th receive aperture, with $j \in \{1, 2, \dots, N_T\}$ and $l \in \{1, 2, \dots, N_R\}$, denoted by a complex channel gain $h_{l,j}$, which is modeled as [36]:

$$h_{l,j} \triangleq \frac{\int_{\mathcal{D}_l} G_j(r - \tilde{r}) ds}{\sqrt{2\pi \int_0^{R_0} r |E_j(r)|^2 dr}}, \quad (1)$$

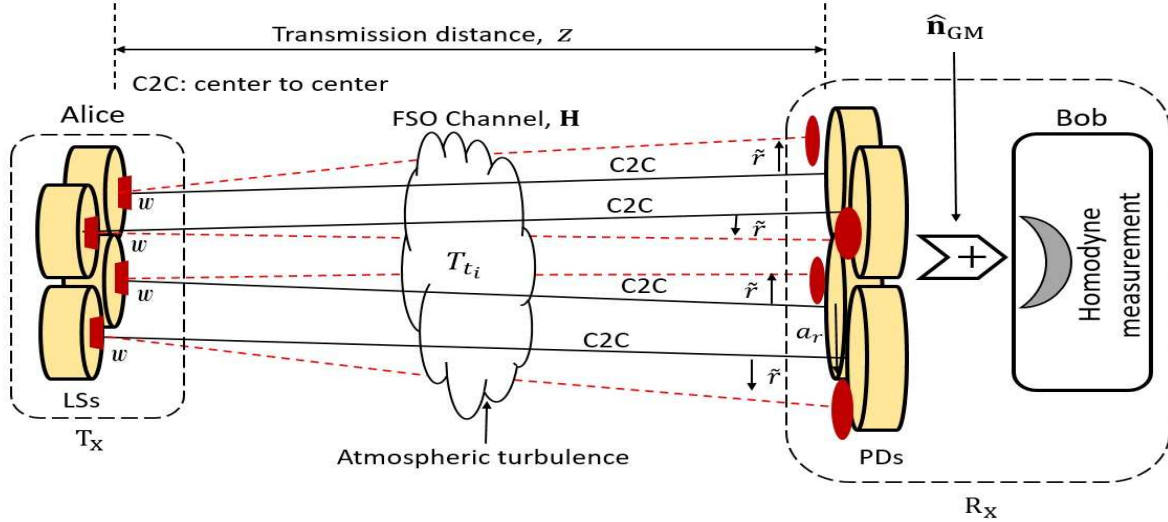


Fig. 1: The considered MIMO FSO CV-QKD system model.

where \mathcal{D}_l covers the receiver's reception area, $E_j(r)$ is the field distribution at the transmitting aperture, expressed as:

$$E_j(r) \triangleq \sqrt{\frac{2}{\pi w^2}} e^{-\frac{r^2}{w^2}}, \quad (2)$$

and $G_j(r)$ denotes the field reaching to l -th receiver aperture, which is given as follows:

$$G_j(r) = 2\pi \int_0^{\rho_{\max}} \rho F_j(\rho) J_0(2\pi r \rho) e^{j\sqrt{k^2 - (2\pi\rho)^2}z} d\rho. \quad (3)$$

In the latter expression, $R_0 \triangleq \sqrt{N_T}w$ is the radius of the transmitter aperture, w is the waist size of the Gaussian beam at the transmitter's sub-apertures, $k \triangleq 2\pi/\lambda$, $\rho_{\max} \triangleq \sin(\frac{\lambda}{\pi w})/\lambda$, a_r is the radius of a PD's lens, λ is the wavelength, and z is the transmission distance between Alice and Bob. Furthermore, $F_j(\rho)$ in (3) outputs the spatial frequency spectrum of $E_j(r)$, and is obtained as follows:

$$F_j(\rho) \triangleq 2\pi \int_0^{R_0} r E_j(r) J_0(2\pi r \rho) dr. \quad (4)$$

It is noted that in (1) the field reaching the aperture of the receiver can be expressed as $G_j(r - \tilde{r})$, with the term \tilde{r} arising due to the misalignment factor of the FSO system. As shown in Fig. 1, misalignment can occur due to the following two key factors: *i*) pointing errors, which may arise from mechanical vibrations or tracking imperfections; and *ii*) beam wandering, resulting from variations in atmospheric conditions. Both these factors determine the equivalent radial standard deviation of the beam centroid displacement, $\sigma_{\tilde{r}}$. Assuming that these factors are independent of each other, $\sigma_{\tilde{r}}$ is computed as:

$$\sigma_{\tilde{r}} \triangleq \sqrt{\sigma_p^2 + \sigma_{TB}^2}, \quad (5)$$

where $\sigma_p^2 \triangleq (\theta_p z)^2$ represents the variance due to the pointing error, θ_p denotes the pointing jitter, and $\sigma_{TB}^2 \triangleq 0.1337\lambda^2 z^2 w^{-1/3} r_c^{-5/3}$ represents the variance arising due to the beam wandering effect, with $r_c = (0.423 k^2 C_n^2 z)^{-3/5}$ denoting the Fried parameter [37]–[39]. Further, C_n^2 refers

to the refractive index structure constant, which measures the level of turbulence following the Kolmogorov model. Generally, C_n^2 ranges from $10^{-14} \text{ m}^{-2/3}$ (indicating moderate turbulence) to $10^{-17} \text{ m}^{-2/3}$ (indicating weak turbulence) [40]. The displacement due to the misalignment factor typically follows a Weibull distribution [41], implying that the probability density function (p.d.f.) of \tilde{r} is mathematically expressed as:

$$f_{\tilde{r}}(v) \triangleq \frac{v}{\sigma_{\tilde{r}}^2} \exp\left(-\frac{v^2}{2\sigma_{\tilde{r}}^2}\right), \quad v \geq 0. \quad (6)$$

Let the singular value decomposition (SVD) of the channel matrix generated using (1) be expressed as $\mathbf{H} = \mathbf{U}\mathbf{\Sigma}\mathbf{V}^\dagger$, where $\mathbf{U} \in \mathbb{C}^{N_R \times N_R}$ and $\mathbf{V} \in \mathbb{C}^{N_T \times N_T}$ are unitary matrices, with the diagonal matrix $\mathbf{\Sigma} \in \mathbb{R}^{N_R \times N_T}$ given as

$$\mathbf{\Sigma} \triangleq \begin{bmatrix} \text{diag}(\sqrt{\beta_1}, \dots, \sqrt{\beta_{r_H}}) & \mathbf{0}_{N_T \times (N_T - r_H)} \\ \mathbf{0}_{(N_R - r_H) \times r_H} & \mathbf{0}_{(N_R - r_H) \times (N_T - r_H)} \end{bmatrix}, \quad (7)$$

where $r_H \leq \min(N_T, N_R)$ is the rank of \mathbf{H} and the entries $\sqrt{\beta_i}$ s, representing the transmittance of each i -th sub-channel ($i = 1, \dots, r_H$), are the non-zero singular values of \mathbf{H} . It is noted that the channel model in (1) incorporates the effect of Gaussian beam propagation, beam spreading, beam wandering, and the effect of the pointing error. However, apart from these effects, the transmittance of the FSO channel also depends on the atmospheric absorption, turbulence-induced fading, and detector efficiency. Thus, the effective transmissivity of each i -th sub-channel can be modified as follows:

$$T_i \triangleq \eta T_{a_i} T_{t_i} \beta_i, \quad (8)$$

where $T_{a_i} \triangleq 10^{-\frac{\delta}{10}z}$ represents the attenuation due to atmospheric absorption, δ (in dB/m) is the attenuation coefficient, and η denotes the detection efficiency at the receiver end. Additionally, T_{t_i} captures the random fading caused by atmospheric turbulence for each i -th transmission path. Experimental results have shown that for long-distance quantum links,

this random turbulence-induced fading follows a lognormal distribution [42], implying that its p.d.f. is given by:

$$f_{T_i}(t_i) \triangleq \frac{1}{t_i \sqrt{2\pi\sigma^2}} \exp\left(-\frac{\left(\ln(t_i) + \frac{\sigma^2}{2}\right)^2}{2\sigma^2}\right), \quad (9)$$

where the parameter σ^2 represents the log-irradiance variance, characterizing the strength of turbulence, and is given by"

$$\sigma^2 \triangleq \exp\left(\frac{0.49\chi^2}{\left(1 + 0.18d^2 + 0.56\chi^{12/5}\right)^{7/6}} + \frac{0.51\chi^2}{\left(1 + 0.9d^2 + 0.62d^2\chi^{12/5}\right)^{5/6}}\right) - 1, \quad (10)$$

where $\chi^2 \triangleq 1.23C_n^2 k^{7/6} z^{11/6}$ and $d \triangleq a_r \sqrt{k/z}$.

B. Additive Noise Model

Apart from the atmospheric effect, the transmission of secret keys encoded using CV-QKD results in an additive noise occurring at the receiver end. For each i -th sub-channel, the noise, denoted by n_{GM_i} , follows the distribution of hybrid quantum noise, whose p.d.f. is derived from a Poisson–Gaussian mixture model [43], [31]. This implies that we can express $n_{GM_i} = n_{p,i} + n_{g,i}$, where $n_{p,i}$ represents the quantum Poisson noise and $n_{g,i}$ indicates the classical additive white Gaussian noise (AWGN). The Poisson component models photon-counting noise due to background radiation and shot noise, while the Gaussian component captures thermal noise, electronic noise, and excess noise introduced by imperfect detectors. Such a Poisson–Gaussian noise model is standard in low-light optical and quantum receivers [44]. Thus, the probability mass function (p.m.f.) of $n_{p,i}$ is given by

$$f_{p,i}(k, \lambda_0) \triangleq \frac{e^{-\lambda_0} \lambda_0^k}{k!}, \quad \lambda_0 \geq 0, k \in \{0, 1, \dots, \infty\}. \quad (11)$$

Furthermore, $n_{g,i}$ follows a Gaussian distribution with mean μ_g and variance σ_g^2 , implying that $n_{g,i} \sim \mathcal{N}(\mu_g, \sigma_g^2) \forall i = 1, \dots, r_H$. Thus, the distribution of the hybrid quantum noise n_{GM_i} can be computed as the convolution of the distributions of $n_{p,i}$ and $n_{g,i}$, yielding the expression:

$$f_{n_{GM_i}}(n) \triangleq \sum_{k=0}^{\infty} \frac{e^{-\lambda_0} \lambda_0^k}{k! \sqrt{2\pi\sigma_g^2}} \exp\left(-\frac{(n - k - \mu_g)^2}{2\sigma_g^2}\right). \quad (12)$$

III. ONE- AND TWO-WAY MIMO CV-QKD PROTOCOLS

This section describes the considered one- and two-way protocols with their corresponding secret key transmission and reception mechanisms. In both protocols, the secret keys are transmitted by using the CV-QKD scheme, and Eve attempts to steal them applying a collective Gaussian attack. This attack is known to be the most comprehensive and effective attack strategy among the class of Gaussian protocols [45].

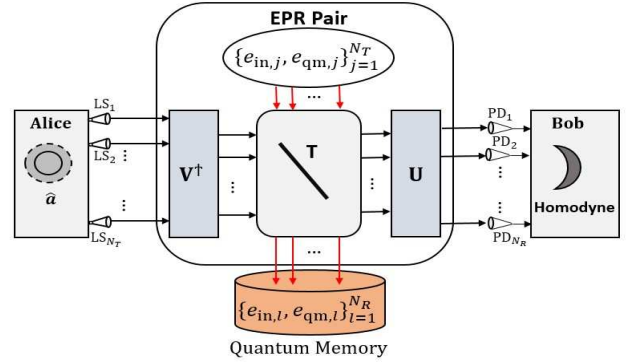


Fig. 2: The MIMO FSO CV-QKD system model employing the one-way protocol.

A. One-Way Protocol

As depicted in Fig. 2, in the one-way MIMO FSO communication system, Alice employs a Gaussian-modulated CV-QKD scheme to securely send secret keys to the legitimate receiver Bob. This transmission occurs over \mathbf{H} that is vulnerable to eavesdropping, and thus, can be fully accessed by Eve. In this protocol, Alice prepares and transmits coherent states as $a_j \triangleq Q_{A,j} + jP_{A,j} \forall j = 1, \dots, N_T$ from her N_T LSs. Here, Q_A and P_A represent the position and momentum quadratures, respectively, at Alice's end. These quadratures are sampled independently from a zero-mean Gaussian distribution with a variance of V_s , implying that $Q_A, P_A \sim \mathcal{N}(0, V_s)$, with $\mathbf{E}[Q_A^2] = \mathbf{E}[P_A^2] = V_s$. Following this, Alice encodes her signals using the precoding matrix \mathbf{V} , while Bob employs the combining operation \mathbf{U}^\dagger at their receiver to recover the secret keys. Further, the eavesdropper, Eve, executes a collective Gaussian attack for which a commonly utilized model is the entangling cloner, in which Eve prepares an Einstein–Podolsky–Rosen (EPR) state, denoted as $\rho_{e_{in}e_{qm}}$, as her quantum ancilla. This state represents a two-mode, zero-mean entangled Gaussian state, completely characterized by its covariance matrix, which is expressed as follows:

$$\Xi_{e_{in}e_{qm}} \triangleq \begin{bmatrix} \nu \mathbf{I}_2 & \sqrt{\nu^2 - 1} \mathbf{Z} \\ \sqrt{\nu^2 - 1} \mathbf{Z} & \nu \mathbf{I}_2 \end{bmatrix}, \quad (13)$$

where $\nu \geq 1$ is the variance of each mode (namely e_{in} and e_{qm}) in the EPR state.

To compromise the transmission of the secret keys, Eve utilizes the collective Gaussian attack by coupling one mode from her EPR pair, referred to as $\hat{e}_{in} \triangleq [\hat{e}_{in,1}, \dots, \hat{e}_{in,N_T}]^T$, with the input coherent state vector $\hat{\mathbf{a}} \triangleq [\hat{a}_1, \dots, \hat{a}_{N_T}]^T$. This is accomplished through a series of beam splitters characterized by the transmittance parameters $\{T_i\}_{i=1}^{r_H}$, which interact with the signals transmitted by Alice post using the precoding matrix \mathbf{V} . These beam splitters yield two distinct outputs for each input mode: *i*) the *legitimate channel output* which undergoes a unitary transformation \mathbf{U}^\dagger at Bob's receiver end; and *ii*) the *eavesdropper's output*, denoted by e_o , which is stored in Eve's quantum memory along with the retained EPR mode e_q . Eve delays her collective measurement until after Alice and Bob have concluded their classical communication phase,

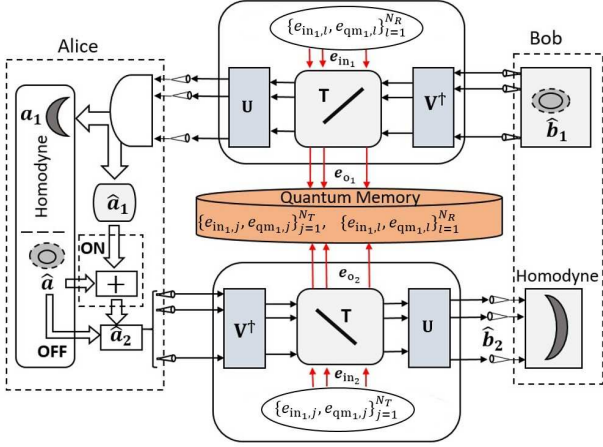


Fig. 3: The MIMO FSO CV-QKD system model with the two-way protocol.

thereby optimizing her information gain. Thus, the effective mode transformation at Bob's receiver can be represented as:

$$\hat{\mathbf{b}} \triangleq \mathbf{U}^\dagger \mathbf{H} \mathbf{V} \hat{\mathbf{a}} + \mathbf{U}^\dagger \mathbf{U} \mathbf{S} \hat{\mathbf{e}}_{\text{in}} + \mathbf{U}^\dagger \hat{\mathbf{n}}_{\text{GM}}, \quad (14)$$

where $\hat{\mathbf{b}} \triangleq [\hat{b}_1, \dots, \hat{b}_{N_R}]^T$ is the received quantum state vector, $\hat{\mathbf{n}}_{\text{GM}} \triangleq [\hat{n}_{\text{GM}_1}, \dots, \hat{n}_{\text{GM}_{N_R}}]^T$ is the additive hybrid noise vector, and $\mathbf{S} \in \mathbb{R}^{N \times N}$ is given by ($N \triangleq \min\{N_T, N_R\}$):

$$\mathbf{S} \triangleq \text{diag} \left(\sqrt{1-T_1}, \dots, \sqrt{1-T_{r_H}}, \mathbf{1}_{(N-r_H)} \right). \quad (15)$$

Applying the SVD of \mathbf{H} in (15) and the overall transmissivity of the FSO channels in (8), the input-output relation for each i -th link between Alice and Bob is obtained as:

$$\hat{b}_i = \sqrt{T_i} \hat{a}_i + \sqrt{1-T_i} \hat{e}_{\text{in}_i} + \hat{n}_{\text{GM}_i} \quad \forall i = 1, \dots, r_H. \quad (16)$$

Additionally, Eve's output for each i -th link is given by:

$$\hat{e}_{o_i} = -\sqrt{1-T_i} \hat{a}_i + \sqrt{T_i} \hat{e}_{\text{in}_i} \quad \forall i = 1, \dots, r_H. \quad (17)$$

B. Two-Way Protocol

The system setup for the one-way protocol can be modified to implement a two-way protocol for quantum communications, as shown in Fig. 3. The two-way quantum communication protocol improves secure key distribution by utilizing bidirectional quantum channels between the legitimate parties. To implement this protocol, Alice and Bob are both equipped with LSs and PDs and, unlike the one-way protocol, Bob begins the process by transmitting N_R Gaussian-modulated thermal coherent states $b_{1,l} \triangleq X_{b_{1,l}} + jP_{b_{1,l}} \quad \forall l = 1, \dots, N_R$ to Alice by utilizing a precoder matrix \mathbf{V} . Here, $X_{b_{1,l}}$ and $P_{b_{1,l}}$ are the position and momentum quadratures, respectively, following respectively the zero-mean Gaussian distributions $X_{b_{1,l}}, P_{b_{1,l}} \sim \mathcal{N}(0, V_s)$. The signal mode travels via the quantum channel and reaches Alice, where she employs a combiner matrix \mathbf{U}^\dagger to the receiving signal mode, which receives the noisy signal modes, denoted as $a_{1,i}$ s. During this transmission, Eve uses the Gaussian collective attack to steal the secret keys by following a process similar to the one

described in the one-way protocol. Thus, the received signal modes at Alice are given as follows:

$$\hat{a}_{1,i} = \sqrt{T_i} \hat{b}_{1,i} + \sqrt{1-T_i} \hat{e}_{\text{in}_{1,i}} + \hat{n}_{\text{GM}_i}^{(1)} \quad \forall i = 1, \dots, r_H, \quad (18)$$

where $\hat{n}_{\text{GM}_i}^{(1)}$ is the hybrid noise at Alice's end. On the other hand, Eve's received signal mode is given as

$$\hat{e}_{o_{1,i}} = -\sqrt{1-T_i} \hat{b}_{1,i} + \sqrt{T_i} \hat{e}_{\text{in}_{1,i}} \quad \forall i = 1, \dots, r_H. \quad (19)$$

Following this phase, Alice can randomly choose between two configurations, namely the **ON** and **OFF** configurations for secret key transmission to Bob. In the **ON** configuration, Alice creates her Gaussian states as $a_i = Q_{a,i} + jP_{a,i}$, where $Q_{a,i}$ and $P_{a,i}$ are random values drawn from a Gaussian distribution with zero mean and a variance of V_s . She then transmits the updated mode as $\hat{a}_{2,i} = \hat{a}_{1,i} + \hat{a}_i \quad \forall i = 1, \dots, r_H$, back to Bob's end. On the contrary, in the **OFF** configuration, Alice performs a homodyne measurement on the incoming quantum states from Bob. Following this measurement, she prepares new coherent states represented by $\hat{a}_{2,i} = \hat{a}_i \quad \forall i = 1, \dots, r_H$ and transmits them to Bob. At the receiving end, Bob applies his detection technique to the incoming mode.

At the conclusion of the two-way quantum communication phase, Alice and Bob perform classical post-processing over an authenticated public channel. In this phase, Alice announces the configuration, i.e., either **ON** or **OFF**, that was selected in each round of the secret key exchange. Furthermore, both parties disclose which quadratures were measured by their respective detection technique. This public exchange enables them to identify the correlated measurement outcomes. In the **OFF** configuration, Alice and Bob acquire two independent sets of correlated variables, denoted as $\{a_{1,i}, b_{1,i}\}_{i=1}^{r_H}$ and $\{a_{2,i}, b_{2,i}\}_{i=1}^{r_H}$. In contrast, in the **ON** configuration, they obtain a single correlated pair $\{a_i, b_i\}_{i=1}^{r_H}$, where Bob's variable b_i is constructed from the linear combination of $b_{1,i}$ and $b_{2,i}$ is obtained during the Bob-to-Alice and Alice-to-Bob signal transmissions, respectively.

The **ON** configuration has been shown to remain effective even in regimes where one-way communication protocols fail [29], [46]. For this reason, we assume Alice selects this configuration and, in the second phase of transmission, she applies the precoding matrix \mathbf{V} to encode her quantum states, while Bob employs the combining matrix \mathbf{U}^\dagger for signal recovery. As in the previous phase, the communication channel remains vulnerable to eavesdropping, and the signal modes received by Bob are modeled accordingly to reflect this potential interception, which is given as follows:

$$\hat{b}_{2,i} = \sqrt{T_i} \hat{a}_{2,i} + \sqrt{1-T_i} \hat{e}_{\text{in}_{2,i}} + \hat{n}_{\text{GM}_i}^{(2)} \quad \forall i = 1, \dots, r_H, \quad (20)$$

where $\hat{n}_{\text{GM}_i}^{(2)}$ is the hybrid noise at Bob's end in the i -th sub-channel. Moreover, Eve's received signal is obtained as:

$$\hat{e}_{o_{2,i}} = -\sqrt{1-T_i} \hat{a}_{2,i} + \sqrt{T_i} \hat{e}_{\text{in}_{2,i}} \quad \forall i = 1, \dots, r_H. \quad (21)$$

IV. ANALYSIS OF THE MUTUAL INFORMATION

The performance of the MIMO FSO CV-QKD systems under consideration is henceforth characterized with respect to their SKRs. The computation of the SKR involves the

computation of the classical mutual information between Alice and Bob, which is analytically assessed for both the one- and two-way protocols in this section.

A. One-Way Protocol

At the receiver end in the CV-QKD system when employing the one-way protocol, Bob employs homodyne detection on each received signal mode \hat{b}_i (recall $i = 1, \dots, r_H$), given in (16), resulting in the following output with $a_i \sim \mathcal{N}(0, V_s)$:

$$b_i^{1\text{-way}} = \sqrt{T_i} a_i + n_{\text{GM}_i}^{1\text{-way}}, \quad (22)$$

where the term $n_{\text{GM}_i}^{1\text{-way}} = \sqrt{T} a_0 + \sqrt{1-T_i} e_{\text{in}_i} + n_{\text{GM}_i}$ is the effective additive noise, with a_0 representing the vacuum thermal noise at Alice following a zero-mean Gaussian distribution with a variance of V_0 (i.e., $a_0 \sim \mathcal{N}(0, V_0)$), and $e_{\text{in}_i} \sim \mathcal{N}(0, \nu)$ being the eavesdropping signal. Using these statistics and the statistics of the hybrid quantum noise given in (12), the p.d.f. of $n_{\text{GM}_i}^{1\text{-way}}$ can be obtained as follows:

$$f_{n_{\text{GM}_i}^{1\text{-way}}}(n) = \sum_{k=0}^{\infty} \frac{e^{-\lambda_0} \lambda_0^k}{k! \sqrt{2\pi\sigma_{n_i,1\text{-way}}^2}} \exp\left(-\frac{(n-k-\mu_g)^2}{2\sigma_{n_i,1\text{-way}}^2}\right), \quad (23)$$

where $\sigma_{n_i,1\text{-way}}^2 = T_i V_0 + (1-T_i)\nu + \sigma_g^2$. Thus, from (22) and (23), the p.d.f. of the received signal at Bob's end is given by

$$f_{b_i^{1\text{-way}}}(b) = \sum_{k=0}^{\infty} \frac{e^{-\lambda_0} \lambda_0^k}{k! \sqrt{2\pi\sigma_{b_i,1\text{-way}}^2}} \exp\left(-\frac{(b-k-\mu_g)^2}{2\sigma_{b_i,1\text{-way}}^2}\right), \quad (24)$$

where $\sigma_{b_i,1\text{-way}}^2 = T_i V_a + (1-T_i)\nu + \sigma_g^2$ and $V_a = V_s + V_0$.

Following the latter derivations, the classical mutual information between the transmitted signal a_i and the received signal $b_i^{1\text{-way}}$, denoted by $I(a_i; b_i^{1\text{-way}})$, can be computed as:

$$\begin{aligned} I(a_i; b_i^{1\text{-way}}) &= h(a_i) + h(b_i^{1\text{-way}}) - h(a_i, b_i^{1\text{-way}}) \\ &= h(a_i) + h(b_i^{1\text{-way}}) - (h(b_i^{1\text{-way}}|a_i) + h(a_i)) \\ &= h(b_i^{1\text{-way}}) - h(\sqrt{T_i} a_i + n_{\text{GM}_i}^{1\text{-way}}|a_i) \\ &= h(b_i^{1\text{-way}}) - h(n_{\text{GM}_i}^{1\text{-way}}), \end{aligned} \quad (25)$$

where $h(b_i^{1\text{-way}})$ and $h(n_{\text{GM}_i}^{1\text{-way}})$ denote the differential entropies of the received signal $b_i^{1\text{-way}}$ and the effective additive noise $n_{\text{GM}_i}^{1\text{-way}}$ for each i -th sub-channel, respectively. The quantities are analytically derived as follows:

$$\begin{aligned} h(b_i^{1\text{-way}}) &= -\int_{-\infty}^{\infty} f_{b_i^{1\text{-way}}}(b) \log(f_{b_i^{1\text{-way}}}(b)) db \\ &= -\int_{-\infty}^{\infty} \left(\sum_{k=0}^{\infty} \frac{e^{-\lambda_0} \lambda_0^k}{k! \sqrt{2\pi\sigma_{b_i,1\text{-way}}^2}} e^{-\frac{(b-k-\mu_g)^2}{2\sigma_{b_i,1\text{-way}}^2}} \right) \\ &\quad \times \log\left(\sum_{k=0}^{\infty} \frac{e^{-\lambda_0} \lambda_0^k}{k! \sqrt{2\pi\sigma_{b_i,1\text{-way}}^2}} e^{-\frac{(b-k-\mu_g)^2}{2\sigma_{b_i,1\text{-way}}^2}} \right) db, \end{aligned} \quad (26)$$

$$\begin{aligned} h(n_{\text{GM}_i}^{1\text{-way}}) &= -\int_{-\infty}^{\infty} f_{n_{\text{GM}_i}^{1\text{-way}}}(n) \log(f_{n_{\text{GM}_i}^{1\text{-way}}}(n)) dn \\ &= -\int_{-\infty}^{\infty} \left(\sum_{k=0}^{\infty} \frac{e^{-\lambda_0} \lambda_0^k}{k! \sqrt{2\pi\sigma_{n_i,1\text{-way}}^2}} e^{-\frac{(n-k-\mu_g)^2}{2\sigma_{n_i,1\text{-way}}^2}} \right) \\ &\quad \times \log\left(\sum_{k=0}^{\infty} \frac{e^{-\lambda_0} \lambda_0^k}{k! \sqrt{2\pi\sigma_{n_i,1\text{-way}}^2}} e^{-\frac{(n-k-\mu_g)^2}{2\sigma_{n_i,1\text{-way}}^2}} \right) dn. \end{aligned} \quad (27)$$

It can be observed from (26) and (27) that the differential entropies involve infinite summations of weighted exponential functions; thus, their numerical evaluation can be mathematically intractable. To this end, we next present tight bounds on these expressions, leading to a bound on the system's mutual information. We particularly perform the definitions:

$$h_L(n_{\text{GM}_i}^{1\text{-way}}) \leq h(n_{\text{GM}_i}^{1\text{-way}}) \leq h_U(n_{\text{GM}_i}^{1\text{-way}}), \quad (28a)$$

$$h_L(b_i^{1\text{-way}}) \leq h(b_i^{1\text{-way}}) \leq h_U(b_i^{1\text{-way}}). \quad (28b)$$

A bound on $I(a_i; b_i^{1\text{-way}})$ can be obtained as follows:

$$\begin{aligned} h_L(n_{\text{GM}_i}^{1\text{-way}}) &\leq h(n_{\text{GM}_i}^{1\text{-way}}) \leq h_U(n_{\text{GM}_i}^{1\text{-way}}) \\ \implies -h_L(n_{\text{GM}_i}^{1\text{-way}}) &\geq -h(n_{\text{GM}_i}^{1\text{-way}}) \geq -h_U(n_{\text{GM}_i}^{1\text{-way}}) \\ \implies h(b_i^{1\text{-way}}) - h_L(n_{\text{GM}_i}^{1\text{-way}}) &\geq h(b_i^{1\text{-way}}) - h(n_{\text{GM}_i}^{1\text{-way}}) \\ &\geq h(b_i^{1\text{-way}}) - h_U(n_{\text{GM}_i}^{1\text{-way}}) \\ \implies h_U(b_i^{1\text{-way}}) - h_L(n_{\text{GM}_i}^{1\text{-way}}) &\geq h(b_i^{1\text{-way}}) - h_L(n_{\text{GM}_i}^{1\text{-way}}) \\ &\geq h(b_i^{1\text{-way}}) - h(n_{\text{GM}_i}^{1\text{-way}}) \\ &= I(a_i; b_i^{1\text{-way}}). \end{aligned} \quad (29)$$

Furthermore, the expressions for $h_U(b_i^{1\text{-way}})$ and $h_L(n_{\text{GM}_i}^{1\text{-way}})$ can be respectively derived using [47, Theorems 2,3] as:

$$\begin{aligned} h_U(b_i^{1\text{-way}}) &= \sum_{k=0}^{\infty} \frac{e^{-\lambda_0} \lambda_0^k}{k!} \left(-\log_2 \left(\frac{e^{-\lambda_0} \lambda_0^k}{k!} \right) \right. \\ &\quad \left. + \frac{1}{2} \log_2(2\pi e \sigma_{b_i,1\text{-way}}^2) \right), \end{aligned} \quad (30)$$

$$\begin{aligned} h_L(n_{\text{GM}_i}^{1\text{-way}}) &= -\sum_{k=0}^{\infty} \left[\frac{e^{-\lambda_0} \lambda_0^k}{k!} \log_2 \left(\sum_{\ell=0}^{\infty} \frac{e^{-\lambda_0} \lambda_0^\ell}{\ell! \sqrt{4\pi\sigma_{n_i,1\text{-way}}^2}} \right. \right. \\ &\quad \left. \left. \times \exp\left(-\frac{(k-\ell)^2}{4\sigma_{n_i,1\text{-way}}^2}\right) \right) \right]. \end{aligned} \quad (31)$$

Substituting (30) and (31) in (29), and performing some algebraic simplifications, the following upper bound on the

mutual information for the MIMO FSO CV-QKD system employing the one-way protocol is obtained:

$$\begin{aligned}
I_B(a_i; b_i^{1\text{-way}}) &= \sum_{k=0}^{\infty} \frac{e^{-\lambda_0} \lambda_0^k}{k!} \left(-\log_2 \left(\frac{e^{-\lambda_0} \lambda_0^k}{k!} \right) \right. \\
&+ \frac{1}{2} \log_2 (2\pi e (T_i V_a + (1 - T_i) \nu + \sigma_g^2)) \\
&+ \log_2 \left(\sum_{\ell=0}^{\infty} \frac{e^{-\lambda_0} \lambda_0^\ell}{\ell! 2 \sqrt{\pi (T_i V_0 + (1 - T_i) \nu + \sigma_g^2)}} \right. \\
&\left. \left. \times \exp \left(-\frac{(k - \ell)^2}{4 (T_i V_0 + (1 - T_i) \nu + \sigma_g^2)} \right) \right) \right). \quad (32)
\end{aligned}$$

B. Two-Way Protocol

For the case where the considered MIMO FSO CV-QKD system employs the **ON** configuration with the two-way protocol, the received signal mode at Bob is given in (20). Then, this node employs the homodyne detection to each received signal mode $\hat{b}_{2,i}$, which is then followed by the post processing of subtracting the input modulation $b_{1,i}$ to generate the effective variable b_i [46], as follows $\forall i = 1, \dots, r_H$:

$$\begin{aligned}
b_i &= b_{2,i} - T_i b_{1,i} \\
&= \sqrt{T_i} a_i + T_i b_0 + \sqrt{1 - T_i} \left(\sqrt{T_i} e_{\text{in}_{1,i}} + e_{\text{in}_{2,i}} \right) \\
&\quad + \sqrt{T_i} n_{\text{GM}_i}^{(1)} + n_{\text{GM}_i}^{(2)}, \quad (33)
\end{aligned}$$

where $n_{\text{GM}_i}^{(1)}$ and $n_{\text{GM}_i}^{(2)}$ are considered to be statistically independent of each other. This expression can be re-written as:

$$b_i = \sqrt{T_i} a_i + n_{\text{GM}_i}^{2\text{-way}}, \quad (34)$$

where $n_{\text{GM}_i}^{2\text{-way}} = \sqrt{(1 - T_i)} (\sqrt{T_i} e_{\text{in}_{1,i}} + e_{\text{in}_{2,i}}) + \sqrt{T_i} a_0 + T_i b_0 + \sqrt{T_i} n_{\text{GM}_i}^{(1)} + n_{\text{GM}_i}^{(2)}$ represents the effective hybrid quantum noise arising from Alice's and Bob's vacuum thermal noise, the eavesdropping signals, and hybrid quantum noise in the two-way framework, with $b_0 \sim \mathcal{N}(0, V_0)$. From the statistics of all the involved terms, the p.d.f. of $n_{\text{GM}_i}^{2\text{-way}}$ can be obtained as follows:

$$\begin{aligned}
f_{n_{\text{GM}_i}^{2\text{-way}}}(n) &= \sum_{k=0}^{\infty} \frac{e^{-\lambda_0} \lambda_0^k}{k! \sqrt{2\pi \sigma_{n_i, 2\text{-way}}^2}} \\
&\times \exp \left(-\frac{(n - k - (1 + \sqrt{T_i}) \mu_g)^2}{2\sigma_{n_i, 2\text{-way}}^2} \right), \quad (35)
\end{aligned}$$

where $\sigma_{n_i, 2\text{-way}}^2 = (T_i + T_i^2) V_0 + (1 - T_i^2) \nu + (1 + T_i^2) \sigma_g^2$. Moreover, the p.d.f. of the received signal at Bob's end can be computed using (34) and (25) as:

$$\begin{aligned}
f_{b_i^{2\text{-way}}}(b) &= \sum_{k=0}^{\infty} \frac{e^{-\lambda_0} \lambda_0^k}{k! \sqrt{2\pi \sigma_{b_i, 2\text{-way}}^2}} \\
&\times \exp \left(-\frac{(b - k - (1 + \sqrt{T_i}) \mu_g)^2}{2\sigma_{b_i, 2\text{-way}}^2} \right), \quad (36)
\end{aligned}$$

where $\sigma_{b_i, 2\text{-way}}^2 = T_i V_a + T_i^2 V_0 + (1 - T_i^2) \nu + (1 + T_i^2) \sigma_g^2$. It is noted that the expressions (35) and (36) are similar to those obtained for the one-way protocol in Section III.A. Thus,

we can similarly compute the upper bound on the differential entropy of $b_i^{2\text{-way}}$, denoted by $h_U(b_i^{2\text{-way}})$, and the lower bound on the differential entropy of $n_{\text{GM}_i}^{2\text{-way}}$, denoted by $h_L(n_{\text{GM}_i}^{2\text{-way}})$:

$$\begin{aligned}
h_U(b_i^{2\text{-way}}) &= \sum_{k=0}^{\infty} \frac{e^{-\lambda_0} \lambda_0^k}{k!} \left(-\log_2 \left(\frac{e^{-\lambda_0} \lambda_0^k}{k!} \right) \right. \\
&\left. + \frac{1}{2} \log_2 (2\pi e \sigma_{b_i, 2\text{-way}}^2) \right), \quad (37)
\end{aligned}$$

$$\begin{aligned}
h_L(n_{\text{GM}_i}^{2\text{-way}}) &= - \sum_{k=0}^{\infty} \left[\frac{e^{-\lambda_0} \lambda_0^k}{k!} \log_2 \left(\sum_{\ell=0}^{\infty} \frac{e^{-\lambda_0} \lambda_0^\ell}{\ell! \sqrt{4\pi \sigma_{n_i, 2\text{-way}}^2}} \right. \right. \\
&\left. \left. \times \exp \left(-\frac{(k - \ell)^2}{4\sigma_{n_i, 2\text{-way}}^2} \right) \right) \right]. \quad (38)
\end{aligned}$$

Using the latter expressions, the following upper bound on the mutual information between the transmitted signal a_i and the received signal $b_i^{2\text{-way}}$ for the MIMO FSO CV-QKD system, for the case where the two-way protocol is used, is deduced:

$$\begin{aligned}
I_B(a_i; b_i^{2\text{-way}}) &= \sum_{k=0}^{\infty} \frac{e^{-\lambda_0} \lambda_0^k}{k!} \left(-\log_2 \left(\frac{e^{-\lambda_0} \lambda_0^k}{k!} \right) + \frac{1}{2} \log_2 (2\pi e \right. \\
&\times (T_i V_a + T_i^2 V_0 + (1 - T_i^2) \nu + (1 + T_i) \sigma_g^2)) \\
&+ \log_2 \left(\sum_{\ell=0}^{\infty} \frac{e^{-\lambda_0} \lambda_0^\ell}{\ell! 2 \sqrt{\pi (T_i^2 V_0 + (1 - T_i^2) \nu + (1 + T_i) \sigma_g^2)}} \right. \\
&\left. \left. \times \exp \left(-\frac{(k - \ell)^2}{4 (T_i^2 V_0 + (1 - T_i^2) \nu + (1 + T_i) \sigma_g^2)} \right) \right) \right). \quad (39)
\end{aligned}$$

V. SKR ANALYSIS UNDER HYBRID QUANTUM NOISE

In response to Eve's Gaussian collective attack, Bob employs homodyne detection along with RR to correct any errors that may occur during transmission. Notably, the RR protocol ensures a positive SKR even in the low-transmissivity regime of $T_i \in [0, 1]$ [20] (high-loss). Following this setup, in this section, analytical SKR expression for both one- and two-way MIMO FSO CV-QKD systems are presented.

A. One-Way MIMO FSO CV-QKD

The effective SKR for each i -th ($i = 1, \dots, r_H$) channel between Alice and Bob for secret key exchange with the one-way protocol is expressed as follows:

$$\begin{aligned}
\text{SKR}_i^{1\text{-way}} &\triangleq \beta I(a_i; b_i^{1\text{-way}}) - \chi(e_i; b_i^{1\text{-way}}) \\
&\approx \beta I_B(a_i; b_i^{1\text{-way}}) - \chi(e_i; b_i^{1\text{-way}}), \quad (40)
\end{aligned}$$

where β is the reconciliation efficiency factor and $I_B(a_i; b_i^{1\text{-way}})$ is given in (32). In addition, $\chi(e_i; b_i^{1\text{-way}})$

denotes the Holevo information [20] between e_i and $b_i^{1\text{-way}}$, which is given by:

$$\begin{aligned} \chi(e_i; b_i^{1\text{-way}}) &\triangleq S(e_i) - S(e_i|b_i^{1\text{-way}}) \\ &= \sum_{q=1}^2 h_o(\lambda_{i_q}^{1\text{-way}}) - \sum_{q=3}^4 h_o(\lambda_{i_q}^{1\text{-way}}), \end{aligned} \quad (41)$$

where $S(e_i)$ and $S(e_i|b_i^{1\text{-way}})$ represent the Von Neumann entropy of Eve's ancillary state, which she stores in her quantum memory, and the conditional Von Neumann entropy of Eve's ancillary state given Bob's quadrature mode b_i . Both of these entropies depend on the symplectic eigenvalues, denoted as λ_q 's (≥ 0), derived from the covariance matrix of the corresponding Gaussian states. Furthermore, the function $h_o(\cdot)$ used to calculate the Von Neumann entropy of a Gaussian quantum state is defined as follows [20]:

$$h_o(\lambda_q) \triangleq \frac{\lambda_q + 1}{2} \log_2 \left(\frac{\lambda_q + 1}{2} \right) - \frac{\lambda_q - 1}{2} \log_2 \left(\frac{\lambda_q - 1}{2} \right). \quad (42)$$

Corresponding to each i -th link, Eve's ancillary state comprises the two modes $e_{\text{qm},i}$ and $e_{o,i}$. The related covariance matrix for these modes, denoted as $\Xi_{E_i}^{1\text{-way}}$, is given as:

$$\Xi_{E_i}^{1\text{-way}} \triangleq \begin{bmatrix} \Lambda_i(\nu, V_a) \mathbf{I}_2 & c_i \mathbf{Z} \\ c_i \mathbf{Z}^T & \nu \mathbf{I}_2 \end{bmatrix}, \quad (43)$$

where $\Lambda_i(\nu, V_a) \triangleq T_i \nu + (1 - T_i) V_a$, $V_a \triangleq V_s + V_0$, and $c_i \triangleq \sqrt{T_i(\nu^2 - 1)}$. The symplectic eigenvalues of this matrix are determined as the absolute values of the eigenvalues of $j\Omega \Xi_{E_i}^{1\text{-way}}$, where $\Omega \in \mathbb{R}^{2n \times 2n}$ is defined, for an n -mode system, as follows:

$$\Omega \triangleq \bigoplus_{j=1}^n \omega = \mathbf{I}_n \otimes \omega, \quad \text{with } \omega = \begin{bmatrix} 0 & 1 \\ -1 & 0 \end{bmatrix}. \quad (44)$$

Additionally, the conditional covariance matrix $\Xi_{E_i|b_i}^{1\text{-way}}$ is:

$$\Xi_{E_i|b_i}^{1\text{-way}} = \Xi_{E_i}^{1\text{-way}} - \frac{1}{V_{b_i}^{1\text{-way}}} \Sigma_i^{1\text{-way}} \mathbf{\Pi} \left(\Sigma_i^{1\text{-way}} \right)^T, \quad (45)$$

where $V_{b_i}^{1\text{-way}} \triangleq T_i V_a + (1 - T_i) \nu + \lambda_0 + \sigma_g^2$ is the variance of the Bob's receiver signal b_i , $\Xi_{E_i}^{1\text{-way}}$ is given in (43), and $\mathbf{\Pi}$ and $\Sigma_i^{1\text{-way}}$ are defined as:

$$\mathbf{\Pi} \triangleq \begin{bmatrix} 1 & 0 \\ 0 & 0 \end{bmatrix}, \quad \Sigma_i^{1\text{-way}} = \begin{bmatrix} \delta_{1,i} \mathbf{I}_2 \\ \delta_{2,i} \mathbf{Z} \end{bmatrix}, \quad (46)$$

where $\delta_{1,i} \triangleq \sqrt{T_i(1 - T_i)}(\nu - V_a)$ and $\delta_{2,i} \triangleq \sqrt{(1 - T_i)(\nu^2 - 1)}$. The symplectic eigenvalues can be derived from the latter results, and can be then used to obtain the analytical expression (47) for the effective SKR of the one-way system (top of the next page).

B. Two-Way MIMO FSO CV-QKD

For the two-way protocol, we consider that Alice chooses the ON configuration, in which she transmits a newly generated signal along with the originally received signal from Bob. When Bob receives this signal, he performs homodyne

detection and RR. The SKR for each i -th LS and PD link between Alice and Bob is expressed as follows:

$$\text{SKR}_i^{2\text{-way}} \approx \beta I_B(a_i; b_i^{2\text{-way}}) - \chi(e_i; b_i^{2\text{-way}}), \quad (48)$$

where $I_B(a_i; b_i^{2\text{-way}})$ is computed in (39) and the Holevo information is given as

$$\chi(e_i; b_i^{2\text{-way}}) = \sum_{q=1}^4 h_o(\lambda_{i_q}^{2\text{-way}}) - \sum_{q=5}^8 h_o(\lambda_{i_q}^{2\text{-way}}). \quad (49)$$

In this expression, $\lambda_{i_q}^{2\text{-way}}$'s represent the symplectic eigenvalues of the covariance matrix of Eve's overall quantum state, which comprises the modes $e_{o_1,i}$, $e_{\text{qm}_1,i}$, $e_{o_2,i}$, and $e_{\text{qm}_2,i}$. These eigenvalues can be determined in a manner analogous to that used in the one-way system. To this end, the covariance matrix of all quantum states available to Eve can be obtained as [46]:

$$\Xi_{E_i}^{2\text{-way}} \triangleq \begin{bmatrix} \sigma_{11_i} \mathbf{I}_2 & c_i \mathbf{Z} & \sigma_{21_i} \mathbf{I}_2 & \mathbf{0}_2 \\ c_i \mathbf{Z}^T & \nu \mathbf{I}_2 & \bar{c}_i \mathbf{Z} & \mathbf{0}_2 \\ \sigma_{21_i} \mathbf{I}_2 & \bar{c}_i \mathbf{Z}^T & \sigma_{22_i} \mathbf{I}_2 & c_i \mathbf{Z} \\ \mathbf{0}_2 & \mathbf{0}_2 & c_i \mathbf{Z}^T & \nu \mathbf{I}_2 \end{bmatrix}, \quad (50)$$

where

$$\begin{aligned} \sigma_{11_i} &\triangleq (1 - T_i) V_a + T_i \nu, \\ \sigma_{21_i} &\triangleq \sqrt{T_i} (1 - T_i) (V_a - \nu), \\ \bar{c}_i &\triangleq - (1 - T_i) \sqrt{(\nu^2 - 1)}, \\ \sigma_{22_i} &\triangleq (1 - T_i^2) V_a + (1 - T_i + T_i^2) \nu \\ &\quad + (1 - T_i) (\lambda_0 + \sigma_g^2). \end{aligned} \quad (51)$$

Additionally, the conditional covariance matrix of Eve's quantum states for each i -th double connection between Alice and Bob can be calculated in a manner akin to (45), as follows:

$$\Xi_{E_i|b_i}^{2\text{-way}} = \Xi_{E_i}^{2\text{-way}} - \frac{1}{V_{b_i}^{2\text{-way}}} \Sigma_i^{2\text{-way}} \mathbf{\Pi} \left(\Sigma_i^{2\text{-way}} \right)^T, \quad (52)$$

where Bob's variance is given by $V_{b_i}^{2\text{-way}} = T_i V_a + T_i^2 V_0 + (1 - T_i^2) \nu + (1 + T_i) \lambda_0 + (1 + T_i) \sigma_g^2$ and the term $\Sigma_i^{2\text{-way}}$ is:

$$\Sigma_i^{2\text{-way}} \triangleq \begin{bmatrix} (T_i \sqrt{1 - T_i} (\nu - V_0)) \mathbf{I}_2 \\ (\sqrt{T_i} (1 - T_i) (\nu^2 - 1)) \mathbf{Z} \\ -\sqrt{T_i} (1 - T_i) \zeta_i \mathbf{Z} \\ (\sqrt{(1 - T_i)} (\nu^2 - 1)) \mathbf{I}_2 \end{bmatrix}, \quad (53)$$

where $\zeta_i \triangleq V_a + T_i (V_0 - \nu) + \lambda_0 + \sigma_g^2$.

The latter derivations can be used to calculate the symplectic eigenvalues of the covariance matrices and the conditional covariance matrix of Eve's modes, and consequently, yield the analytical expression (54) for the effective SKR of the two-way system (top of the next page).

C. Asymptotic Analysis

We herein focus on the limit of high modulation, i.e., $V_s \gg V_0, \nu, \sigma_g^2$. For this case, the expression (32) for the

$$\text{SKR}_{\text{MIMO}}^{1\text{-way}} = \sum_{i=1}^{r_H} \mathbf{E}_{T_i} \left[\text{SKR}_i^{1\text{-way}} \right] \approx \sum_{i=1}^{r_H} \mathbf{E}_{T_i} \left[\beta I_B \left(a_i; b_i^{1\text{-way}} \right) - \sum_{q=1}^2 h_o \left(\lambda_{i_q}^{1\text{-way}} \right) + \sum_{q=3}^4 h_o \left(\lambda_{i_q}^{1\text{-way}} \right) \right] \quad (47)$$

$$\text{SKR}_{\text{MIMO}}^{2\text{-way}} = \sum_{i=1}^{r_H} \mathbf{E}_{T_i} \left[\text{SKR}_i^{2\text{-way}} \right] \approx \sum_{i=1}^{r_H} \mathbf{E}_{T_i} \left[\beta I_B \left(a_i; b_i^{2\text{-way}} \right) - \sum_{q=1}^4 h_o \left(\lambda_{i_q}^{2\text{-way}} \right) + \sum_{q=5}^8 h_o \left(\lambda_{i_q}^{2\text{-way}} \right) \right] \quad (54)$$

mutual information between Alice and Bob, when the one-way protocol is used, can be approximated as follows:

$$\begin{aligned} & I_B \left(a_i; b_i^{1\text{-way}} \right) \\ & \approx \sum_{k=0}^{\infty} \frac{e^{-\lambda_0} \lambda_0^k}{k!} \left(-\log_2 \left(\frac{e^{-\lambda_0} \lambda_0^k}{k!} \right) + \frac{1}{2} \log_2 (2\pi e T_i V_s) \right) \\ & + \log_2 \left(\sum_{\ell=0}^R \frac{e^{-\lambda_0} \lambda_0^\ell}{\ell! 2 \sqrt{\pi (T_i V_0 + (1 - T_i) \nu + \sigma_g^2)}} \right. \\ & \left. \times \exp \left(-\frac{(k - \ell)^2}{4 (T_i V_0 + (1 - T_i) \nu + \sigma_g^2)} \right) \right). \quad (55) \end{aligned}$$

In addition, the symplectic eigenvalues of Eve's covariance in (43) and the conditional covariance matrix in (46) can be approximated as follows:

$$\begin{aligned} \lambda_{i_1}^{1\text{-way}} & \approx \nu, & \lambda_{i_2}^{1\text{-way}} & \approx (1 - T_i) V_s, \\ \lambda_{i_3}^{1\text{-way}} & \approx \nu, & \lambda_{i_4}^{1\text{-way}} & \approx \sqrt{\frac{(1 - T_i) V_s \nu}{T_i}}. \quad (56) \end{aligned}$$

Using the latter approximations along with the asymptotic expression of $h_0(x) \approx \log_2 \left(\frac{e x}{2} \right)$ for $x \gg 1$, the Holevo information in (41) can be also approximated as:

$$\chi \left(e_i; b_i^{1\text{-way}} \right) \approx \frac{1}{2} \log_2 \left(\frac{T_i (1 - T_i) V_s}{\nu} \right). \quad (57)$$

With the latter approximations and after performing some algebraic manipulations, an asymptotic expression for the SKR performance of the considered one-way MIMO FSO CV-QKD system is obtained as in (58) (top of the next page).

Similarly, the expression (39) for the mutual information between Alice and Bob for the case of the two-way protocol is approximated as follows:

$$\begin{aligned} & I_B \left(a_i; b_i^{2\text{-way}} \right) \\ & \approx \sum_{k=0}^{\infty} \frac{e^{-\lambda_0} \lambda_0^k}{k!} \left(-\log_2 \left(\frac{e^{-\lambda_0} \lambda_0^k}{k!} \right) + \frac{1}{2} \log_2 (2\pi e T_i V_s) \right) \\ & + \log_2 \left(\sum_{\ell=0}^R \frac{e^{-\lambda_0} \lambda_0^\ell}{\ell! 2 \sqrt{\pi (T_i^2 V_0 + (1 - T_i^2) \nu + (1 + T_i) \sigma_g^2)}} \right. \\ & \left. \times \exp \left(-\frac{(k - \ell)^2}{4 (T_i^2 V_0 + (1 - T_i^2) \nu + (1 + T_i) \sigma_g^2)} \right) \right). \quad (59) \end{aligned}$$

Moreover, the symplectic eigenvalues of Eve's covariance matrix in (50) and the conditional covariance matrix in (52) are approximated as:

$$\begin{aligned} \lambda_{i_1}^{2\text{-way}} & \approx \lambda_{i_2}^{2\text{-way}} \approx \nu, & \lambda_{i_3}^{2\text{-way}} \lambda_{i_4}^{2\text{-way}} & \approx (1 - T_i)^2 V_s^2, \\ \lambda_{i_5}^{2\text{-way}} & \approx \nu, & \lambda_{i_6}^{2\text{-way}} & \approx \sqrt{\frac{((1 + T_i^3) \nu + (1 - T_i) T_i^2 V_0 \nu^2)}{(1 - T_i) T_i^2 V_0 + (1 + T_i^3) \nu}}, \\ \lambda_{i_7}^{2\text{-way}} \lambda_{i_8}^{2\text{-way}} & \approx \sqrt{\frac{V_s^3 (1 - T_i)^3 ((1 - T_i) T_i^2 V_0 + (1 + T_i^3) \nu)}{T_i}}, \quad (60) \end{aligned}$$

yielding the following approximation for the Holevo information in (49):

$$\begin{aligned} \chi \left(e_i; b_i^{2\text{-way}} \right) & \approx \frac{1}{2} \log_2 \left(\frac{T_i (1 - T_i) V_s}{T_i^2 V_0 + \nu + T_i^3 (\nu - V_0)} \right) \\ & + h_0(\nu) - h_o \left(\lambda_{i_6}^{2\text{-way}} \right). \quad (61) \end{aligned}$$

Using all above, an asymptotic expression for the SKR performance of the considered two-way MIMO FSO CV-QKD system is given as in (62) (top of the next page).

Without loss of generality, we also assert the importance of investigating a scenario where Eve's variance is precisely set to $\nu = 1$ and the thermal noise variance V_0 closely aligns with ν , i.e., $V_0 \approx \nu$ [20], [48]. This consideration is pivotal for a comprehensive understanding of the system's dynamics when variances are comparable. Using (58) and (62), the difference between the SKRs obtained for the one- and two-way MIMO FSO systems for CV-QKD can be computed as in (63) (top of the next page). Furthermore, for $T_i \ll 1 \forall i = 1, \dots, r_H$, the differential SKR in (63) can be further simplified as:

$$\Delta \text{SKR}_{\text{MIMO}} \Big|_{\{T_i\}_{i=1}^{r_H} \ll 1} \approx \frac{1}{2} \sum_{i=1}^{r_H} \mathbf{E}_{T_i} \left[\log_2 (1 + T_i^2 V_0) \right]. \quad (64)$$

It is noted that T_i 's can be considered as statistically independent. Thus, the differential gain obtained by using the two-way protocol over the one-way one is proportional to r_H . This indicates that increasing the MIMO configuration results in SKR gains for the considered FSO CV-QKD system.

VI. NUMERICAL RESULTS AND DISCUSSION

This section presents the numerical results that corroborate the analytical framework presented in this paper. We have considered the following system parameters for carrying out the numerical investigation: $N_T = N_R = r_H$, $\lambda = 1550$ nm, $w = 2.5$ mm, $a_r = 10$ cm, $c = 3 \times 10^8$ m/s, $T_o = 296$ K, $h = 6.63 \times 10^{-34}$ Js, $k_B = 1.38 \times 10^{-23}$ J/K, $\nu = 1$, and $V_s = 10^3$.

$$\text{SKR}_{\text{MIMO}}^{\text{1-way}} \approx \sum_{i=1}^{r_H} \mathbf{E}_{T_i} \left[\sum_{k=0}^{\infty} \frac{e^{-\lambda_0} \lambda_0^k}{k!} \left(-\log_2 \left(\frac{e^{-\lambda_0} \lambda_0^k}{k!} \right) + \frac{1}{2} \log_2 (2\pi e T_i^2 V_s) + \log_2 \left[\sum_{\ell=0}^{\infty} \frac{e^{-\lambda_0} \lambda_0^\ell}{\ell! 2\sqrt{\pi} (T_i V_0 + (1-T_i)\nu + \sigma_g^2)} \right] \right. \right. \\ \left. \left. \times \exp \left(-\frac{(k-\ell)^2}{4(T_i V_0 + (1-T_i)\nu + \sigma_g^2)} \right) \right) \right] - \frac{1}{2} \log_2 \left(\frac{T_i(1-T_i)V_s}{\nu} \right) \quad (58)$$

$$\text{SKR}_{\text{MIMO}}^{\text{2-way}} \approx \sum_{i=1}^{r_H} \mathbf{E}_{T_i} \left[\sum_{k=0}^{\infty} \frac{e^{-\lambda_0} \lambda_0^k}{k!} \left(-\log_2 \left(\frac{e^{-\lambda_0} \lambda_0^k}{k!} \right) + \log_2 \left[\sum_{\ell=0}^{\infty} \frac{e^{-\lambda_0} \lambda_0^\ell \times \exp \left(-\frac{(k-\ell)^2}{4(T_i^2 V_0 + (1-T_i^2)\nu + (1+T_i)\sigma_g^2)} \right)}{\ell! 2\sqrt{\pi} (T_i^2 V_0 + (1-T_i^2)\nu + (1+T_i)\sigma_g^2)} \right] \right. \right. \\ \left. \left. + \frac{1}{2} \log_2 (2\pi e T_i^2 V_s) \right) - \frac{1}{2} \log_2 \left(\frac{T_i(1-T_i)V_s}{T_i^2 V_0 + \nu + T_i^3(\nu - V_0)} \right) - h_0(\nu) + h_0(\lambda_{i_6}^{\text{2-way}}) \right] \quad (62)$$

$$\Delta \text{SKR}_{\text{MIMO}} = \text{SKR}_{\text{MIMO}}^{\text{2-way}} - \text{SKR}_{\text{MIMO}}^{\text{1-way}} \\ \approx \sum_{i=1}^{r_H} \mathbf{E}_{T_i} \left[\sum_{k=0}^{\infty} \frac{e^{-\lambda_0} \lambda_0^k}{k!} \left(\log_2 \left[\frac{(1+\sigma_g^2) \sum_{\ell=0}^{\infty} \frac{e^{-\lambda_0} \lambda_0^\ell}{\ell!} \exp \left(\frac{-(k-\ell)^2}{4(1+(1+T_i)\sigma_g^2)} \right)}{(1+(1+T_i)\sigma_g^2) \sum_{\ell=0}^{\infty} \frac{e^{-\lambda_0} \lambda_0^\ell}{\ell!} \exp \left(\frac{-(k-\ell)^2}{4(1+\sigma_g^2)} \right)} \right] \right) + \frac{1}{2} \log_2 (1+T_i^2 V_0) \right] \quad (63)$$

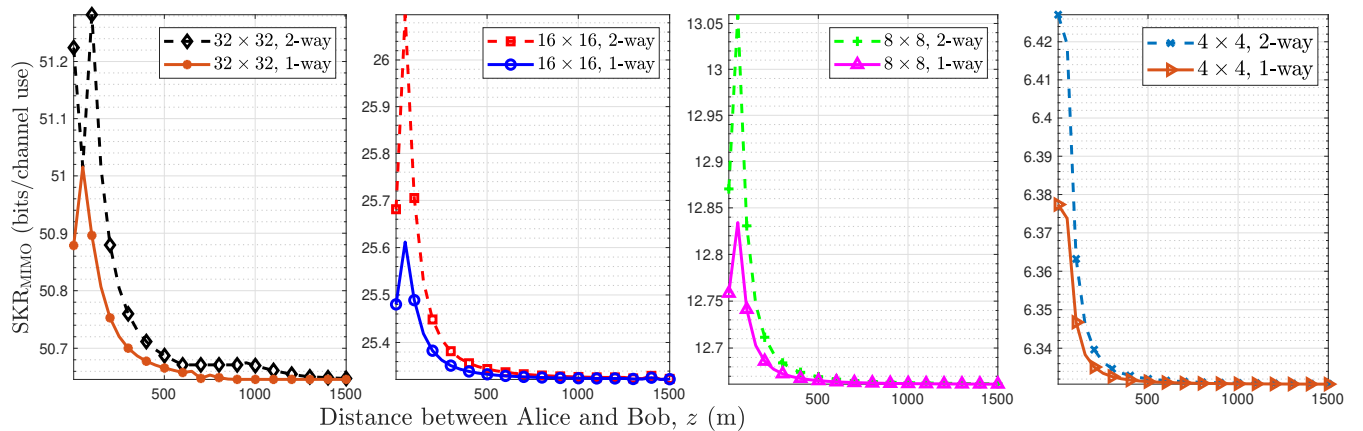


Fig. 4: SKR_{MIMO} vs. distance between Alice and Bob, z , for the MIMO configuration $N_T = N_R = \{4, 8, 16, 32\}$, $\lambda_0 = 1$, $\sigma_g^2 = 0.001$, $\eta = 1$, $\beta = 1$, and $C_n^2 = 10^{-15} \text{m}^{-2/3}$.

Further, $V_0 = 2\bar{n} + 1$, where $\bar{n} = 1/(\exp(hf_c/k_B T_o) - 1)$, $f_c = c/\lambda$, and $\delta = 0.43 \times 10^{-3} \text{ dB/m}$.

Figure 4 presents the plots of the SKR_{MIMO} for both the one- and two-way protocols used with the considered MIMO FSO CV-QKD system under hybrid quantum noise as a function of the transmission distance z between Alice and Bob. It is observed that, across all MIMO configurations, the SKR exhibits a sharp decay over short ranges, eventually transitioning into a shallow, distance-insensitive tail. It is also shown that the two-way protocol consistently outperforms the one-way one, with the relative advantage being most notable at short ranges and gradually narrowing as the distance z increases. As the MIMO order increases, the performance curves rise across all values of z . This trend remains consistent over varying distances, although the added benefits of larger MIMO tend to diminish as the distance increases. This phenomenon can

be attributed to the dominance of path loss and pointing error due to turbulence at longer transmission distances, and to the more performance degradation from hybrid quantum noise in larger MIMO configurations.

It has been observed that the analytical bounds presented in [31] closely follow the numerically evaluated classical mutual information which leads to the same with SKR. This finding indicates a close tightness of the bounds for the considered system model. Finally, it can be seen in Fig. 4 that, within the considered range of transmission distances and MIMO configurations, the analytical bounds reported in [31] closely follow the numerically evaluated SKRs, indicating near-tightness of the bounds in this regime.

Figure 5 illustrates the ratio of the SKR between the two- and one-way protocols for varying MIMO configurations. It can be observed that, across all MIMO sizes, the ratio exceeds

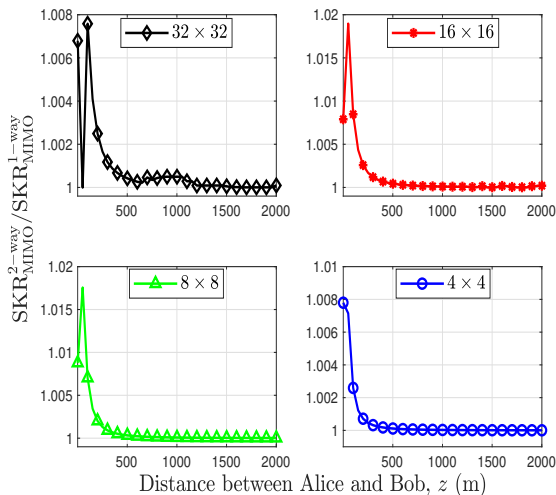


Fig. 5: SKR ratio vs. distance between Alice and Bob, z , for $N_T = N_R = \{4, 8, 16, 32\}$ MIMO configuration, $\lambda_0 = 1$, $\sigma_g^2 = 0.001$, $\eta = 1$, $\beta = 1$, and $C_n^2 = 10^{-15} \text{m}^{-2/3}$.

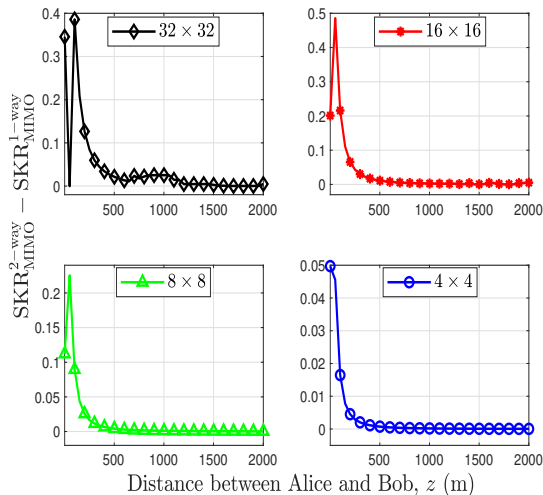


Fig. 6: SKR difference vs. distance between Alice and Bob, z , for $N_T = N_R = \{4, 8, 16, 32\}$, $\lambda_0 = 1$, $\sigma_g^2 = 0.001$, $\eta = 1$, $\beta = 1$, and $C_n^2 = 10^{-15} \text{m}^{-2/3}$.

unity at a short range, indicating a distinct two-way advantage. However, as the distance increases, this ratio quickly diminishes toward unity. Nevertheless, the SKR ratio remains above unity over a longer transmission distance compared to lower MIMO configurations, indicating a monotonic increase in achievable range as the MIMO order increases. It is also depicted that the peak SKR ratio is lower for both very high and very low MIMO configurations than for intermediate ones. This behavior arises because higher-order MIMO systems are more susceptible to inter-channel interference at the receiver, whereas lower-order MIMO systems are less effective at mitigating fading losses and noise effects. Moreover, Fig. 6 depicts the difference in SKRs between the two- and one-way protocols with respect to the distance between Alice and Bob.

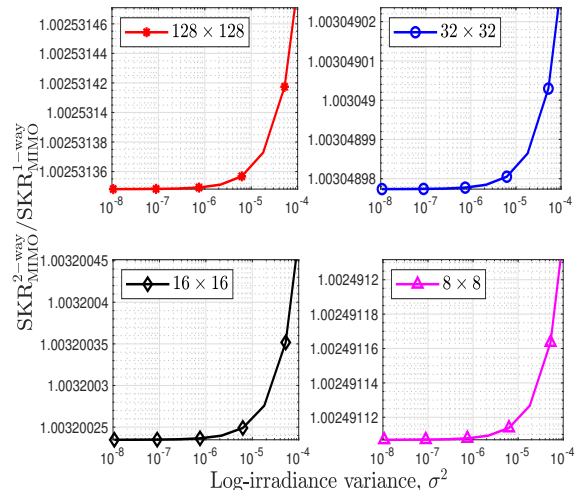


Fig. 7: SKR ratio vs. lognormal irradiance variance, σ^2 , for $N_T = N_R = \{8, 16, 32, 128\}$, $\eta = 1$, $z = 200 \text{ m}$, and $C_n^2 = (10^{-17} - 10^{-14}) \text{m}^{-2/3}$.

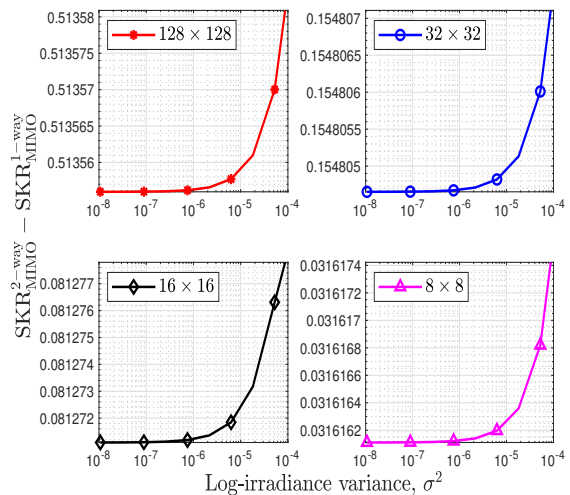


Fig. 8: SKR difference vs. lognormal irradiance variance, σ^2 , for $N_T = N_R = \{8, 16, 32, 128\}$, $\eta = 1$, $z = 200 \text{ m}$, and $C_n^2 = (10^{-17} - 10^{-14}) \text{m}^{-2/3}$.

A similar trend to the SKR ratio is demonstrated, with the SKR difference falling quickly at lower distances and remaining marginally greater than zero at longer distances.

Figure 7 illustrates the relative benefits of the two-way protocol under turbulence via the quantity $\text{SKR}_{\text{MIMO}}^{2\text{-way}} - \text{SKR}_{\text{MIMO}}^{1\text{-way}}$, as a function of the log-irradiance variance σ^2 . It is shown that, for all MIMO setups, the ratio remains above unity for the entire range of σ^2 . The curves show a consistent and convex rise, particularly as the scintillation as $\sigma^2 \geq 10^{-6}$. This indicates that the effect of atmospheric scintillation is not in the same proportion for both protocols, showing that the two-way system is resilient to atmospheric scintillation.

Figure 8 illustrates the differential SKR gain of the two-way protocol over the one-way counterpart, $\Delta \text{SKR}_{\text{MIMO}}$, for

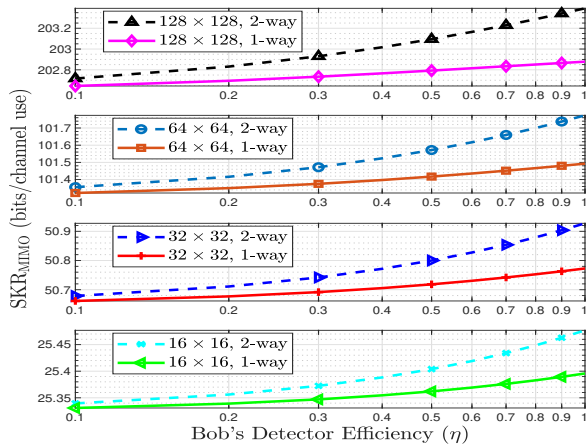


Fig. 9: SKR vs. detector efficiency η for $N_T = N_R = \{16, 32, 64, 128\}$ at $z = 200$ m for hybrid quantum noise parameter $\lambda_0 = 1$, $\sigma_g^2 = 0.001$, and $C_n^2 = 10^{-15} \text{ m}^{-2/3}$.

different σ^2 values reflecting the strength of atmospheric scintillation. The results show that $\Delta\text{SKR}_{\text{MIMO}}$ increases as the MIMO configuration scales up. With respect to σ^2 , this metric remains nearly constant at first, begins to rise when $\sigma^2 \geq 10^{-6}$, and then exhibits only a marginal increase at higher values of σ^2 . This again indicates that the overall impact of atmospheric scintillation on the two-way protocol is weaker than on the one-way protocol.

The metric SKR_{MIMO} as a function of Bob's detector efficiency η for $N_R = N_T = \{16, 32, 64, 128\}$ is plotted in Fig. 9. Each subplot compares the two- and one-way protocols under identical parameter settings. It is demonstrated that, for each MIMO configuration, SKR_{MIMO} exhibits a consistent increase as η rises. Throughout the entire range of η , the two-way protocol performs better than the one-way, with the most noticeable difference occurring at moderate to high efficiency values, i.e., $\eta \geq 0.5$. It can be clearly observed from these plots that the SKR values almost double with a doubling in the MIMO configuration, thus, justifying the result obtained in (64). Furthermore, the sensitivity of the system's SKR to η in terms of the value of $\frac{d\text{SKR}_{\text{MIMO}}}{d\eta}$ increases with the MIMO order. The gains from increasing η are modest at lower MIMO setups but become more significant for the higher ones.

Finally, Fig. 10 illustrates SKR_{MIMO} as a function of SNR for both protocols. It is shown that, in the low SNR range, the curves obtained from the two-way protocol fall below the ones obtained from the one-way counterpart. This is attributed to the additive noise, which has a greater impact in the two-way protocol. Furthermore, the two-way protocol demonstrates stronger sensitivity to SNR, exhibiting a steeper increase compared to one-way systems. In addition, it can be seen that SKR for both protocols saturates at higher SNR values. Higher MIMO system configurations lead to a notable SKR improvement, with λ_0 values consistently increasing across the entire SNR range, as compared to lower MIMO setups.

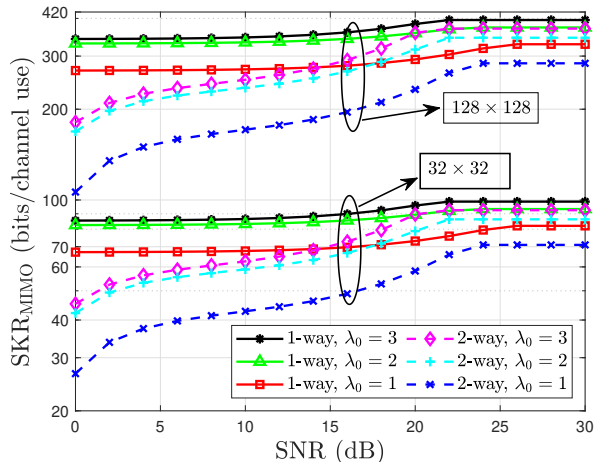


Fig. 10: SKR_{MIMO} vs. SNR (dB) for $N_R = N_T = \{32, 128\}$, $z = 500$ m, $\lambda_0 = \{1, 2, 3\}$, and $T_i = 0.5$.

VII. CONCLUSIONS

This paper presented a MIMO FSO system with two legitimate users, employing CV-QKD for secret key exchange in the presence of an eavesdropper, attempting to jeopardize secure communications through a collective Gaussian attack. The considered FSO channels were subjected to atmospheric turbulence, introducing beam spreading and wandering, pointing error, attenuation, and turbulence-induced fading. The legitimate system was also assumed to be subjected to hybrid quantum noise, degrading CV-QKD performance. A mathematical framework for characterizing the transmissivity of the considered FSO MIMO channel was presented. Furthermore, two protocols, a one-way and a two-way, were proposed for secret key exchange. Owing to the statistics of the hybrid quantum noise, bounds on the mutual information between the coherent states of the eavesdropper and the legitimate receiver were computed for both protocols. In addition, for the case where the legitimate receiver employs homodyne detection and RR, closed-form and asymptotic expressions for the system's SKR for both protocols were derived. Our numerical investigations showcased that the differential gain obtained by employing the two-way protocol over the one-way counterpart is proportional to the rank of the MIMO FSO channel. Increasing the MIMO configuration while using the two-way protocol resulted in improved SKR performance, facilitating secure secret key exchange over larger distances between the legitimate ends.

REFERENCES

- [1] M. Z. Chowdhury, M. Shahjalal, S. Ahmed, and Y. M. Jang, "6G wireless communication systems: Applications, requirements, technologies, challenges, and research directions," *IEEE Open J. Commun. Society*, vol. 1, pp. 957–975, Jul. 2020.
- [2] I. F. Akyildiz, A. Kak, and S. Nie, "6G and beyond: The future of wireless communications systems," *IEEE Access*, vol. 8, pp. 133 995–134 030, Jul. 2020.
- [3] G. Araniti, A. Iera, S. Pizzi, and F. Rinaldi, "Toward 6G non-terrestrial networks," *IEEE Netw.*, vol. 36, no. 1, pp. 113–120, Jan./Feb. 2022.
- [4] P. He, H. Lei, D. Wu, R. Wang, Y. Cui, Y. Zhu, and Z. Ying, "Nonterrestrial network technologies: Applications and future prospects," *IEEE Int. Things J.*, vol. 12, no. 6, pp. 6275–6299, Mar. 2025.

- [5] G. Geraci, D. López-Pérez, M. Benzaghta, and S. Chatzinotas, "Integrating terrestrial and non-terrestrial networks: 3D opportunities and challenges," *IEEE Commun. Mag.*, vol. 61, no. 4, pp. 42–48, Apr. 2023.
- [6] M. M. Azari, S. Solanki, S. Chatzinotas, O. Kodheli, H. Sallouha, A. Colpaert, J. F. Mendoza Montoya, S. Pollin, A. Haqiqatnejad, A. Mostaani, E. Lagunas, and B. Ottersten, "Evolution of non-terrestrial networks from 5G to 6G: A survey," *IEEE Commun. Surveys & Tuts.*, vol. 24, no. 4, pp. 2633–2672, 2022.
- [7] M. Elamassie and M. Uysal, "Free space optical communication: An enabling backhaul technology for 6G non-terrestrial networks," *Photonics*, vol. 10, no. 11, Oct. 2023.
- [8] A. Bekkali, M. Hattori, Y. Hara, and Y. Suga, "Free space optical communication systems for 6G: A modular transceiver design," *IEEE Wireless Commun.*, vol. 30, no. 5, pp. 50–57, Oct. 2023.
- [9] K. P. Peppas, G. C. Alexandropoulos, E. D. Xenos, and A. Maras, "The Fischer–Snedecor \mathcal{F} -distribution model for turbulence-induced fading in free-space optical systems," *J. Lightwave Technol.*, vol. 38, no. 6, pp. 1286–1295, Mar. 2020.
- [10] K. Ikeda, Y. Sato, O. Koyama, and M. Yamada, "Two-dimensional encryption system for secure free-space optical communication of time-series data streams," *Electron. Lett.*, vol. 55, no. 13, pp. 752–754, Jun. 2019.
- [11] W. M. R. Shakir and S. A. A. Mohammed, "Free space optical communications security and reliability trade-off: A survey," in *Proc. Int. Conf. Natural and Applied Sciences*, 2022, pp. 114–119.
- [12] S. A. A. El-Mottaleb, A. G. Mohamed, H. Y. Ahmed, and M. Zeghid, "Performance enhancement of FSO communication system under rainy weather environment using a novel encryption technique," *IEEE Access*, vol. 12, pp. 13 729–13 746, Jan. 2024.
- [13] P. Cao, X. Hu, J. Wu, L. Zhang, X. Jiang, and Y. Su, "Physical layer encryption in OFDM-PON employing time-variable keys from ONUs," *IEEE Photonics J.*, vol. 6, no. 2, pp. 1–6, Apr. 2014.
- [14] H. A. Sharath, J. Vrindavanam, S. Dana, and S. N. Prasad, "Quantum-resilient cryptography: A survey on classical and quantum algorithms," *IEEE Access*, vol. 13, pp. 172 854–172 877, Sep. 2025.
- [15] C. K. Gitonga, "The impact of quantum computing on cryptographic systems: Urgency of quantum-resistant algorithms and practical applications in cryptography," *European J. Inf. Technol. Comp. Science*, vol. 5, no. 1, pp. 1–10, Jan. 2025.
- [16] C. Weedbrook *et al.*, "Gaussian quantum information," *Rev. Mod. Phys.*, vol. 84, no. 2, p. 621, May 2012.
- [17] I. B. Djordjevic, "Optimized-eight-state CV-QKD protocol outperforming Gaussian modulation based protocols," *IEEE Photon. J.*, vol. 11, no. 4, pp. 1–10, Jun. 2019.
- [18] C. Weedbrook, S. Pirandola, and T. C. Ralph, "Continuous-variable quantum key distribution using thermal states," *Phys. Rev. A*, vol. 86, no. 2, p. 022318, Aug. 2012.
- [19] N. K. Kundu, S. P. Dash, M. R. McKay, and R. K. Mallik, "MIMO terahertz quantum key distribution," *IEEE Commun. Lett.*, vol. 25, no. 10, pp. 3345–3349, Oct. 2021.
- [20] C. Weedbrook, S. Pirandola, S. Lloyd, and T. C. Ralph, "Quantum cryptography approaching the classical limit," *Phys. Rev. Lett.*, vol. 105, no. 11, p. 110501, Sep. 2010.
- [21] S. Pirandola, "Limits and security of free-space quantum communications," *Phys. Rev. Res.*, vol. 3, no. 1, p. 013279, May 2021.
- [22] V. Scarani, H. Bechmann-Pasquinucci, N. J. Cerf, M. Dušek, N. Lütkenhaus, and M. Peev, "The security of practical quantum key distribution," *Rev. Mod. Phys.*, vol. 81, pp. 1301–1350, Sep. 2009.
- [23] Z. Yichen, B. Yiming, L. Zhengyu, Y. Song, and G. Hong, "Continuous-variable quantum key distribution system: Past, present, and future," *Appl. Phys. Rev.*, vol. 11, no. 011318, Mar. 2024.
- [24] S. Sahu, A. Lawey, and M. Razavi, "Continuous variable quantum key distribution in multiple-input multiple-output settings," Aug. 2023. [Online]. Available: <https://arxiv.org/abs/2308.11320>.
- [25] S. Pirandola *et al.*, "Advances in quantum cryptography," *Adv. in Opt. and Photon.*, vol. 12, no. 4, pp. 1012–1236, Dec. 2020.
- [26] H. Zhao and M.-S. Alouini, "On the transmission probabilities in quantum key distribution systems over FSO links," *IEEE Trans. Commun.*, vol. 69, no. 1, pp. 429–442, Jan. 2021.
- [27] M. Q. Vu, H. D. Le, T. V. Pham, and A. T. Pham, "Design of satellite-based FSO/QKD systems using GEO/LEOs for multiple wireless users," *IEEE Photon. J.*, vol. 15, no. 4, pp. 1–14, Aug. 2023.
- [28] N. Alshaer and T. Ismail, "Performance evaluation and security analysis of UAV-based FSO/CV-QKD system employing DP-QPSK/CD," *IEEE Photon. J.*, vol. 14, no. 3, pp. 1–11, Jun. 2022.
- [29] S. Pirandola, S. Mancini, S. Lloyd, and S. L. Braunstein, "Continuous-variable quantum cryptography using two-way quantum communication," *Nature Physics*, vol. 4, no. 9, p. 726–730, Jul. 2008.
- [30] P. V. Trinh and A. T. Pham, "Design and secrecy performance of novel two-way free-space QKD protocol using standard FSO systems," in *Proc. IEEE Int. Conf. Commun.*, Paris, France, Jul. 2017.
- [31] M. Chakraborty, A. Mukherjee, I. Krikidis, A. Nag, and S. Chandra, "A hybrid noise approach to modeling of free-space satellite quantum communication channel for continuous-variable QKD," *IEEE Trans. Green Commun. Netw.*, vol. 9, no. 3, pp. 1311–1325, Sep. 2025.
- [32] S. Kumar and S. P. Dash, "RIS-assisted THz MIMO wireless system in the presence of direct link for CV-QKD with limited quantum memory," 2024. [Online]. Available: <https://arxiv.org/abs/2410.16731>
- [33] S. Kumar, S. P. Dash, D. Ghose, and G. C. Alexandropoulos, "RIS-assisted MIMO CV-QKD at THz frequencies: Channel estimation and secret key rate analysis," *IEEE Trans. Commun.*, vol. 73, no. 12, pp. 15 612–15 624, Dec. 2025.
- [34] S. Kumar and S. P. Dash, "SKR analysis of one- and two-way CV-QKD MIMO FSO communication system," *IEEE Commun. Lett.*, vol. 29, no. 10, pp. 2456–2460, Oct. 2025.
- [35] G. C. Alexandropoulos, N. C. Sagias, F. I. Lazarakis, and K. Berberidis, "New results for the multivariate nakagami- m fading model with arbitrary correlation matrix and applications," *IEEE Trans. Wireless Commun.*, vol. 8, no. 1, pp. 245–255, Jan. 2009.
- [36] N. Zhao, X. Li, G. Li, and J. M. Kahn, "Capacity limits of spatially multiplexed free-space communication," *Nature Photonics*, vol. 9, no. 12, pp. 822–826, Dec. 2015.
- [37] Y. Liu and H. Li, "Research on transmission performance of multiple-input multiple-output optical communication in atmospheric turbulence," in *Proc. Int. Conf. Measuring Technol. Mechatronics Autom.*, 2020, pp. 630–633.
- [38] S. Pirandola, "Satellite quantum communications: Fundamental bounds and practical security," *Phys. Rev. Res.*, vol. 3, no. 2, p. 023130, May 2021.
- [39] L. C. Andrews and R. L. Phillips, *Laser Beam Propagation through Random Media*, 2nd ed. Bellingham, WA: SPIE Press, 2005.
- [40] N. K. Kundu, M. R. McKay, R. Murch, and R. K. Mallik, "Intelligent reflecting surface-assisted free space optical quantum communications," *IEEE Trans. Wireless Commun.*, vol. 23, no. 5, pp. 5079–5093, May 2024.
- [41] A. A. Farid and S. Hranilovic, "Outage capacity optimization for free-space optical links with pointing errors," *J. Lightw. Technol.*, vol. 25, no. 7, pp. 1702–1710, Jul. 2007.
- [42] I. Capraro *et al.*, "Impact of turbulence in long range quantum and classical communications," *Phys. Rev. Lett.*, vol. 109, no. 20, p. 200502, Nov. 2012.
- [43] M. Chakraborty, A. Mukherjee, A. Nag, and S. Chandra, "Hybrid quantum noise model to compute Gaussian quantum channel capacity," *IEEE Access*, vol. 12, pp. 14 671–14 689, Jan. 2024.
- [44] H. Kaushal and G. Kaddoum, "Optical communication in space: Challenges and mitigation techniques," *IEEE Commun. Surveys & Tuts.*, vol. 19, no. 1, pp. 57–96, 2017.
- [45] M. Navascués, F. Grosshans, and A. Acín, "Optimality of Gaussian attacks in continuous-variable quantum cryptography," *Phys. Rev. Lett.*, vol. 97, p. 190502, Nov. 2006.
- [46] C. Weedbrook, C. Ottaviani, and S. Pirandola, "Two-way quantum cryptography at different wavelengths," *Phys. Rev. A*, vol. 89, p. 012309, Jan. 2014.
- [47] M. F. Huber, T. Bailey, H. Durrant-Whyte, and U. D. Hanebeck, "On entropy approximation for Gaussian mixture random vectors," in *Proc. 2008 IEEE Int. Conf. Multisensor Fusion Integr. Intell. Syst.*, Seoul, South Korea, Aug. 2008, pp. 181–188.
- [48] C. Ottaviani *et al.*, "Terahertz quantum cryptography," *IEEE J. Sel. Areas Commun.*, vol. 38, no. 3, pp. 483–495, Mar. 2020.